iScience

Article

Actin fenestrae amplify the membrane response to hypertonic stress in osmosensory neurons

Graphical abstract

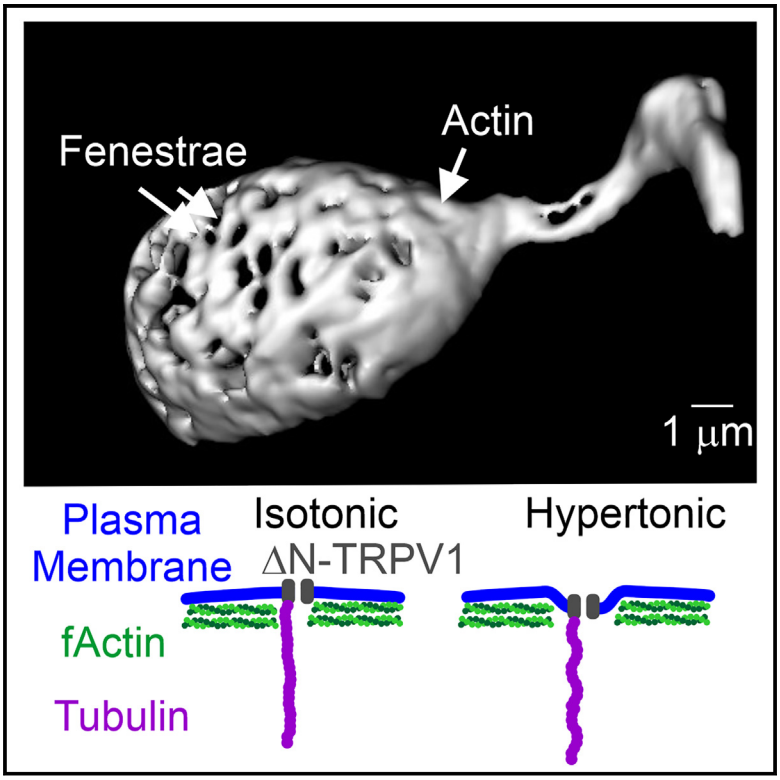

Authors

Anzala Murtaz, Charles W. Bourque

Correspondence

charles.bourque@mcgill.ca

In brief

Molecular biology; Neuroscience; Cell biology

Highlights

- The actin cortex of osmosensory neurons is fenestrated
- Many ΔN-TRPV1 channels attached to microtubules are aligned to fenestrae
- Hypertonic stress induces the formation of plasma membrane pits at fenestrae

Murtaz & Bourque, 2025, iScience *28*, 112042
March 21, 2025
https://doi.org/10.1016/j.isci.2025.112042

CellPress

iScience

CellPress
OPEN ACCESS

Article

Actin fenestrae amplify the membrane response to hypertonic stress in osmosensory neurons

Anzala Murtaz[1] and Charles W. Bourque[1,2,*]
[1]Brain Repair and Integrative Neuroscience Program, Research Institute of the McGill University Health Centre, 1650 Cedar Avenue, Montreal, QC H3G1A4, Canada
[2]Lead contact
*Correspondence: charles.bourque@mcgill.ca
https://doi.org/10.1016/j.isci.2025.112042

SUMMARY

Osmosensory neurons detect hypertonic stress when ΔN-TRPV1 channels are activated through a push force delivered by microtubules during cell shrinking, and this process requires an essential yet unknown contribution from actin filaments. Here, we show that the actin cortex of these neurons feature fenestrations that allow for the formation of pits that magnify the osmotically induced displacement of the plasma membrane compared to that expected from uniform shrinking. Furthermore, we found that many N-terminal variant of the transient receptor potential vanilloid 1 (ΔN-TRPV1) channels attached to microtubules are aligned with fenestrae and such sites undergo greater hypertonicity-induced displacement than predicted by geometrically uniform cell shrinking. These results indicate that actin filaments contribute to the establishment of nanoscale architecture at sites which may optimize osmosensory transduction.

INTRODUCTION

Osmosensory neurons (ONs) detect ongoing changes in plasma osmolality and initiate vital homeostatic responses such as thirst and vasopressin (anti-diuretic hormone) secretion to maintain hydromineral balance.[1–4] When serum osmolality rises above the set point by $\geq$ 1% (i.e., +3 mosmol/kg), ONs become depolarized and thus increase their rate of action potential firing,[5–9] which allows them to command appropriate homeostatic effector responses. This intrinsic osmosensitive process has been shown to require an N-terminal variant of the transient receptor potential vanilloid 1 (ΔN-TRPV1) channel.[10,11] Notably, ΔN-TRPV1 channels are activated as ONs undergo hypertonicity-induced shrinking via a push-force from microtubules, which are physically linked to the ΔN-TRPV1 channels.[12] Another key cytoskeletal element, filamentous actin (f-actin), is also necessary for this process because mechanical and osmotic activation of ONs is abolished by actin depolymerization and amplified by promoting actin polymerization.[13,14] Indeed, ONs feature a prominent layer of subcortical f-actin.[15] However, it is unknown whether f-actin interacts with ΔN-TRPV1 channels and how it contributes to the process of osmosensory transduction.

RESULTS

TRPV1 interacts with tubulin but not actin in ONs

In agreement with previous work showing that ΔN-TRPV1 is specifically expressed in ONs of the supraoptic nucleus (SON) and the organum vasculosum of the lamina terminalis (OVLT),[11] anti-TRPV1 antibodies selectively stained these neurons but not non-osmosensitive neurons of the suprachiasmatic nucleus (SCN; Figures 1A and S1). As expected, proximity ligation assays (PLAs) performed using anti-TRPV1 and anti-Tubulin antibodies revealed puncta along the perimeter of isolated SON[12] and OVLT ONs, but not SCN neurons (Figures 1B, 1C, and S2). To determine if ΔN-TRPV1 channels interact also with actin, we performed PLA on acutely isolated SON ONs using anti-actin and anti-TRPV1 antibodies. Whereas puncta were readily detected along the perimeter of the cells when PLA was performed using anti-TRPV1 and anti-tubulin antibodies (Figures 1B and 1D), puncta were virtually absent when PLA was performed using anti-TRPV1 and anti-actin antibodies (Figure 1E). Indeed, the number of puncta (mean ± SEM) observed along the perimeter in single confocal sections was significantly greater with anti-tubulin (14.18 ± 0.9760; n = 28 cells from 10 rats) than anti-actin (1.087 ± 0.3381; n = 23 cells from 4 rats; $p < 0.0001$, Mann-Whitney test; Figure 1F).

The subcortical actin layer of ONs is fenestrated

These results indicate that ΔN-TRPV1 channels rarely interact with actin compared to tubulin. Therefore, actin's vital role in the mechanoactivation of these channels may be related to its ability to shape plasma membrane (PM) domains that enable this process rather than via a direct physical interaction. Notably, differences in actin density within small sub-domains have been shown to affect membrane shape[16] and elasticity.[17,18] To determine if subcortical actin density is homogeneous or not, we performed high-resolution imaging of ONs isolated from the SON and stained with fluorescent phalloidin, which binds to f-actin. The obtained images revealed that the subcortical actin layer is non-uniform and features segments of high fluorescence interspersed with regions of lower fluorescence (Figures 2A and 2B).

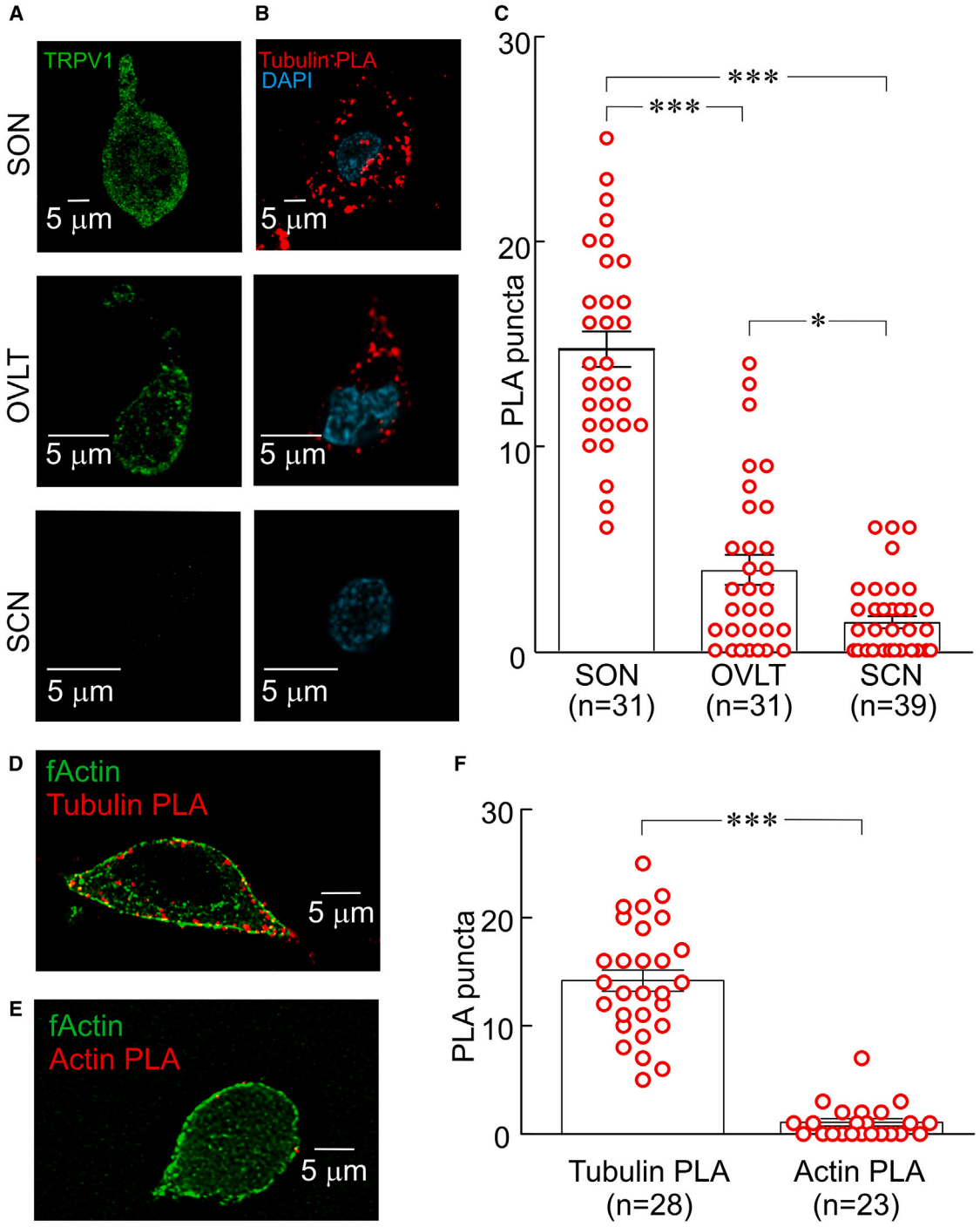

Figure 1. Proximity ligation assays reveal that TRPV1 interacts with tubulin but not actin in osmosensory neurons

(A) Neurons isolated from the supraoptic nucleus (SON), organum vasculosum of the lamina terminalis (OVLT), and suprachiasmatic nucleus (SCN) stained with anti-TRPV1 antibody (green).

(B) Neurons from the SON, OVLT, and SCN with TRPV1-tubulin proximity ligation assay (Tubulin PLA) puncta (red) and DAPI staining (blue).

(C) Bar graphs show the mean (±SEM) number of PLA puncta along the perimeter of single confocal images taken from each cell in SON ($n = 31$), OVLT ($n = 31$), and SCN ($n = 39$ from 4 rats for all nuclei) neurons (each red circle represents an individual cell; one-way ANOVA and Tukey's multiple comparison test; $^{*}p < 0.05$; $^{**}p < 0.01$; $^{***}p < 0.001$).

(legend continued on next page)

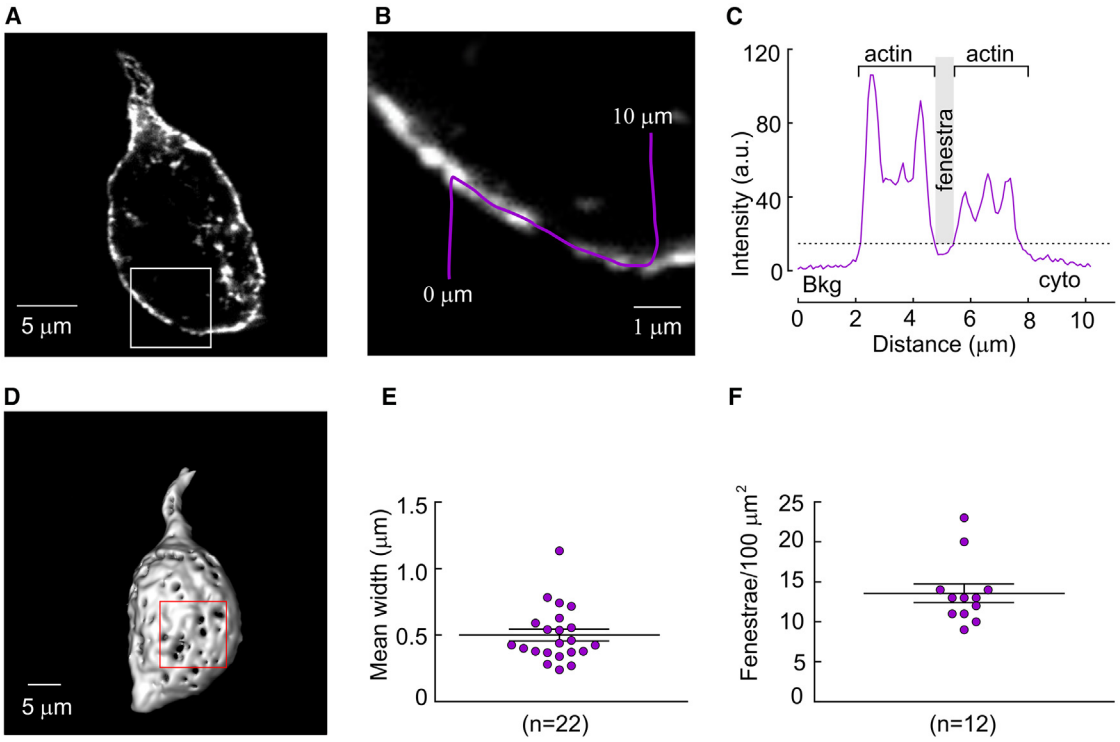

Figure 2. Submembrane actin fenestrae in osmosensory neurons

(A) Isolated SON neuron stained with phalloidin (white). Box shows portion of image magnified in (B). Scale bar indicates 5 μm.

(B) Purple freehand line is drawn from background (0 μm), through subcortical actin, and then into the cytoplasm (10 μm). Scale bar indicates 1 μm.

(C) Profile of phalloidin fluorescence intensity (a.u., arbitrary units) along the purple line in (B). Black dashed line is 10 units above the mean cytoplasmic (cyto) fluorescence. Subcortical regions falling below this line are considered fenestrae (gray bar). Bkg, background.

(D) Image is a 3D rendered ON using phalloidin staining. Red square (100 μm^2) shows area used for density analysis. Scale bar indicates 5 μm.

(E) Scatterplot shows the average width (mean ± SEM; horizontal lines) of 22 fenestrae measured in 5 ONs from 3 rats.

(F) Scatterplot shows the number of actin fenestrae per 100 μm^2 (mean ± SEM) in 12 ONs from 3 rats.

Notably, the intensity of the phalloidin signal in actin-poor zones was barely above cytoplasmic fluorescence (Figures 2B and 2C), suggesting that these actin-poor zones represent gaps in the actin cortex. To characterize the shape and dimensions of these gaps, we 3D rendered high-resolution stacks of single ONs using ImageJ. As observed in Figure 2D, these gaps were ovoid in shape and resembled fenestrae. The mean (±SEM) fenestrae width was 0.50 ± 0.04 μm (n = 22 cells from 3 rats; Figure 2E), and the mean (±SEM) density of fenestrae on the cell surface was 13.6 ± 1.2 fenestrae per 100 μm^2 (n = 12 cells from 3 rats; Figure 2F).

Membrane response to hypertonic stress is intensified at actin fenestrae

Previous work has shown that increases in subcortical actin density enhance membrane stiffness in ONs.[19] We therefore hypothesized that physiologically relevant hypertonic stimuli may induce the formation of pits at sites of fenestrae rather than cause homogeneous shrinking of the entire cell perimeter. To test this hypothesis, we examined the effects of hypertonic stimuli on PM topology using dynamic super-resolution imaging of isolated ONs labeled with a fluorescent membrane dye. In live ONs, bath application of hypertonic saline (+4.5 mosmol/kg) induced the formation of pits that deepened gradually as a function of time (Figure 3A). Analysis of ONs that were fixed with paraformaldehyde 60 s following the application of a hypertonic stimulus revealed the presence of numerous pits, whereas ONs fixed in isotonic solution were devoid of such features. Osmotically induced pits featured a mean width (±SEM) of 0.60 ± 0.04 μm and a mean depth (±SEM) of 0.20 ± 0.01 μm (Figures 3B and 3C), and pit depth increased as a function of width (0.299 ± 0.019; r^2 = 0.248; n = 49; Figure 3D). Indeed, 3D reconstruction of stacks of super-resolution images revealed the presence of pits in hypertonicity-treated ONs but not in those

(D) Image shows SON neuron stained with Tubulin PLA (red puncta) and f-actin stained with fluorescent phalloidin (green).

(E) Image shows SON neuron stained with TRPV1-actin (Actin PLA; red puncta) and f-actin stained with fluorescent phalloidin (green).

(F) Bar graphs show the number of PLA puncta (mean ± SEM) along the perimeter of single confocal images taken from cells treated with Tubulin PLA (n = 28 cells from 10 rats) or with Actin PLA (n = 23 cells from 4 rats; $p < 0.0001$, Mann-Whitney test). Scale bars indicate 5 μm.

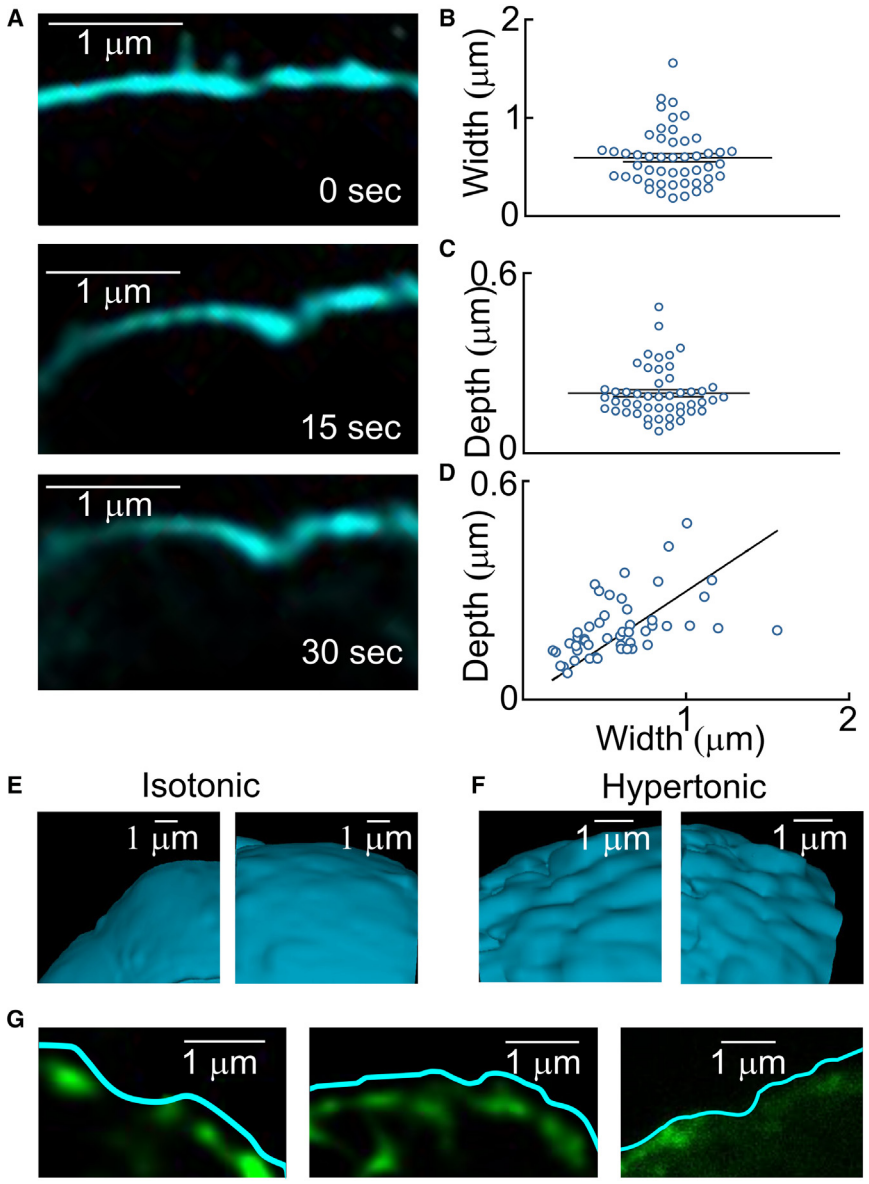

Figure 3. Actin fenestrae amplify membrane response to hypertonic stress

(A) Consecutive super-resolution confocal images (time intervals at lower right) show formation of a local membrane pit in a live ON (cyan, membrane staining) exposed to a +4.5 mosmol/kg stimulus.

(B) Scatterplot shows the average membrane pit width (mean ± SEM) in individual cells exposed to hypertonic stress (n = 49 cells from 6 rats).

(C) Scatterplot shows the average membrane pit depth (mean ± SEM) in individual cells exposed to hypertonic stress (n = 49 cells from 6 rats).

(D) Graph shows the relation between membrane pit width and depth in cells exposed to hypertonic stress. Black line is a linear regression through the data (slope, 0.1463; y-intercept, 0.1125, r^2, 0.2481).

(E) Images show 3D surface topology of two isolated ONs in isotonic conditions.

(F) Images show 3D surface topology of two isolated ONs in hypertonic conditions (+4.5 mosmol/kg).

(G) Three representative super-resolution confocal images of isolated ONs with skeletonized cell membrane (cyan) and live actin probe staining (green). Scale bars indicate 1 μm.

maintained in isotonic solution (Figures 3E and 3F). Moreover, in agreement with our hypothesis, osmotically induced membrane pits were commonly observed at sites of low actin density (Figure 3G).

Tubulin-TRPV1 interaction sites commonly align with actin fenestrae

The formation of membrane pits at actin fenestrae suggests that these sites may be preferentially associated with sites of osmosensory transduction. To test this hypothesis, we examined the distribution of tubulin-TRPV1 PLA sites in isolated ONs in which f-actin was stained with fluorescent phalloidin. Confocal images and 3D reconstruction revealed that PLA sites are commonly aligned with gaps in the actin cortex (Figures 4A–4C). The formation of membrane pits also suggests that membrane displacement at such sites may exceed the predicted displacement associated with geometrically uniform shrinking under hypertonic conditions. For example, in an ON with a diameter of 20 μm, a +4.5 mosmol/kg stimulus would be expected to cause a decrease in cell radius of 48 nm if the volume change was uniform. However, we saw that the average pit depth caused by such a stimulus was five to ten times greater (~250–500 nm; Figures 3C and 4D). ΔN-TRPV1 channels aligned with actin fenestrae may therefore experience amplified osmotically induced displacement (Figure 4E). Indeed, image analysis suggests that the inward displacement of tubulin-TRPV1 PLA puncta is greater at sites where pits are formed compared to those lacking pits (Figures 4F and 4G).

DISCUSSION

Previous work showed that f-actin is essential for osmosensory transduction in ONs.[13,14,20] However, it remained unknown if this reflected a direct interaction with ΔN-TRPV1 channels, or a different mechanism. Our data show that f-actin does not interact with ΔN-TRPV1 channels. Rather, we found that the subcortical actin layer is not uniform but features fenestrae, which enable membrane pit formation under hypertonic stress. Although ONs express membrane reserves and therefore non-uniform surface topology,[21] osmosensory transduction has been heretofore analyzed, assuming uniform volume changes observed using phase-contrast microscopy.[9,10,19,22] Our study

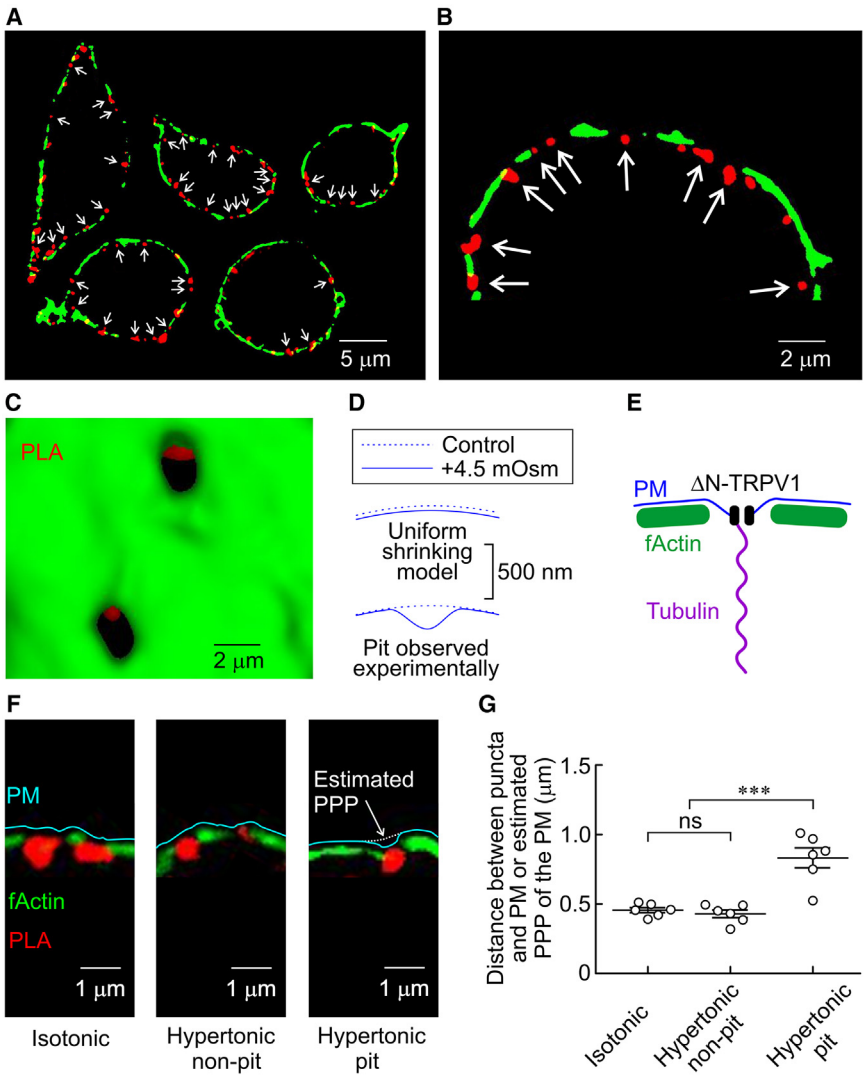

Figure 4. PLA puncta align with actin fenestrae, which magnify osmotically induced PM displacement

(A) Image of isolated ONs treated with tubulin-TRPV1 PLA (red) and fluorescent phalloidin (green). Arrows indicate regions where PLA puncta are aligned with actin fenestrae. Puncta located >1 μm away from the actin cortex were masked for clarity. Scale bar indicates 5 μm.

(B) Magnified image of an ON's actin cortex with PLA puncta within fenestrae indicated by arrows (top middle cell in a). Scale bar indicates 2 μm.

(C) Image shows 3D surface topology of an ON with PLA puncta visible through actin fenestrae. Scale bar indicates 2 μm.

(D) Schematic illustrates the theoretical PM displacement caused by a +4.5 mosmol/kg stimulus assuming uniform cell shrinking, and the PM displacement associated with pit formation observed experimentally.

(E) Hypothetical arrangement of the osmosensory transduction site.

(F) Images show tubulin-TRPV1 PLA puncta in ONs in isotonic conditions or in hypertonic conditions in non-pit and pit domains. Dotted white line indicates estimated PM pre pit position (PPP). Scale bars indicate 1 μm.

(G) Scatterplot shows the distance (mean ± SEM) between PLA puncta and PM (isotonic or hypertonic non-pit) or estimated PPP of the PM (hypertonic pit) in 6 domains for all conditions ($n = 12$ cells from 3 rats; one-way ANOVA and Tukey's multiple comparison test; $^{*}p < 0.05$; $^{**}p < 0.01$; $^{***}p < 0.001$; ns, non-significant).

reveals that the shrinking response of ONs to mild hyperosmotic stimuli is fundamentally non-uniform. Indeed, we found that fenestrae in the actin cortex enable the formation of membrane pits at sites of low actin density, despite a lack of observable reduction in cell radius (Figure 4D). The formation of pits requires the availability of local membrane lipid that can be recruited to form such features because the lipid bilayer cannot simply be stretched to any significant extent.[23] Accordingly, the presence of excess membrane reserves may specifically serve this purpose in ONs.

It remains to be determined whether a fenestrated actin cortex is a unique feature of ONs. However, previous work has shown that some types of neurons appear to lack a subcortical actin layer (e.g., neurons in the cortex or SCN), or display a significantly less dense actin cortex when compared to ON (e.g., hippocampal neurons).[15] Therefore, the actin cortex of other neurons may be less capable of facilitating the formation of inward pits during hypertonic stimulation. Additional work is required to test this hypothesis.

A previous study showed that the activation of ΔN-TRPV1 channels during osmosensory transduction is mediated by a push-force applied via microtubules during cell shrinking.[12,24] The formation of pits may therefore be functionally relevant for osmosensory transduction as it amplifies osmotically induced membrane displacement at actin fenestrae. Indeed, sites at which ΔN-TRPV1 and tubulin interact as detected by PLA were preferentially located in actin fenestrae, indicating that such sites may be specialized for the detection of mild physiological hypertonic stimuli (Figure 4E). A potential concern is the possibility that the lack of phalloidin staining (i.e., at a fenestra) is simply a consequence of molecules associated with PLA puncta hindering the binding of phalloidin to local f-actin. However, sites at which both signals overlapped in single super-resolution confocal image planes could frequently be observed (e.g., Figure 4A).

Interestingly, previous studies have shown that increases in actin density can enhance osmosensory gain.[13,14,19] This observation is somewhat paradoxical because our study suggests that domains lacking actin (i.e., fenestrae) may facilitate or even be required for the detection of mild osmotic stimuli. Therefore, we surmise that conditions leading to a global increase in subcortical actin density[14,15,19] may simultaneously preserve or

enhance fenestrae. Specifically, an increase in the number of fenestrae could provide additional sites for osmosensory transduction. Moreover, the formation of fenestrae of greater width would enhance membrane displacement at individual transduction sites (Figure 3D) and could potentially amplify push-activation of ΔN-TRPV1 channels by microtubules. Additional studies are required to test these hypotheses.

Limitations of the study

Our experiments were performed on acutely disassociated neurons to optimize the spatial resolution of various molecules using confocal microscopy. Further experiments should be performed to verify that similar mechanisms are present and can be detected *in situ*. Although osmotically induced vasopressin secretion is sensitized in pregnant and lactating females, no quantitative differences have been observed under control conditions between males and females. Our study was performed exclusively in male animals. Although we presume that the observations reported here may also apply to control females, it is likely that differences could be observed during gestation and lactation, and this interesting possibility requires further investigation.

RESOURCE AVAILABILITY

Lead contact

Requests for further information and resources should be directed to and will be fulfilled by the lead contact, Dr. Charles W. Bourque (charles.bourque@mcgill.ca).

Materials availability

This study did not generate new materials.

Data and code availability

- All the data reported in this paper will be shared by the lead contact upon request.
- This paper does not report original codes.
- Any additional information required to reanalyze the data reported in this paper is available from the lead contact upon request.

ACKNOWLEDGMENTS

This work was supported by a Project Grant from the Canadian Institutes of Health Research (CIHR; PJT 180511) and an infrastructure grant from the Canada Foundation for Innovation and a James McGill Chair to C.W.B. The Research Institute of the McGill University Health Center (RIMUHC) receives generous funding from the Fonds de Recherche Québec Santé.

AUTHOR CONTRIBUTIONS

A.M.: conceptualization, investigation, data curation, formal analysis, preparation of figures, and writing. C.W.B.: conceptualization, funding acquisition, methodology, project administration, supervision, and writing.

DECLARATION OF INTERESTS

The authors declare no competing interests.

STAR★METHODS

Detailed methods are provided in the online version of this paper and include the following:

SUPPLEMENTAL INFORMATION

Supplemental information can be found online at https://doi.org/10.1016/j.isci.2025.112042.

Received: February 14, 2024
Revised: November 20, 2024
Accepted: February 13, 2025
Published: February 17, 2025

REFERENCES

1. Bourque, C.W. (2008). Central mechanisms of osmosensation and systemic osmoregulation. Nat. Rev. Neurosci. *9*, 519–531. https://doi.org/10.1038/nrn2400.
2. McKinley, M.J., Denton, D.A., Oldfield, B.J., De Oliveira, L.B., and Mathai, M.L. (2006). Water intake and the neural correlates of the consciousness of thirst. Semin. Nephrol. *26*, 249–257. https://doi.org/10.1016/j.semnephrol.2006.02.001.
3. Johnson, A.K., Cunningham, J.T., and Thunhorst, R.L. (1996). Integrative role of the lamina terminalis in the regulation of cardiovascular and body fluid homeostasis. Clin. Exp. Pharmacol. Physiol. *23*, 183–191.
4. Noda, M., and Hiyama, T.Y. (2015). Sodium sensing in the brain. Pflügers Archiv *467*, 465–474. https://doi.org/10.1007/s00424-014-1662-4.
5. Ciura, S., and Bourque, C.W. (2006). Transient receptor potential vanilloid 1 is required for intrinsic osmoreception in organum vasculosum lamina terminalis neurons and for normal thirst responses to systemic hyperosmolality. J. Neurosci. *26*, 9069–9075. https://doi.org/10.1523/JNEUROSCI.0877-06.2006.
6. Vivas, L., Chiaraviglio, E., and Carrer, H.F. (1990). Rat organum vasculosum laminae terminalis *in vitro*: responses to changes in sodium concentration. Brain Res. *519*, 294–300.
7. Mason, W.T. (1980). Supraoptic neurones of rat hypothalamus are osmosensitive. Nature *287*, 154–157.
8. Abe, H., and Ogata, N. (1982). Ionic mechanism for the osmotically-induced depolarization in neurones of the guinea-pig supraoptic nucleus *in vitro*. J. Physiol. *327*, 157–171. https://doi.org/10.1113/jphysiol.1982.sp014225.
9. Oliet, S.H., and Bourque, C.W. (1993). Mechanosensitive channels transduce osmosensitivity in supraoptic neurons. Nature *364*, 341–343. https://doi.org/10.1038/364341a0.
10. Sharif-Naeini, R., Witty, M.F., Seguela, P., and Bourque, C.W. (2006). An N-terminal variant of Trpv1 channel is required for osmosensory transduction. Nat. Neurosci. *9*, 93–98. https://doi.org/10.1038/nn1614.
11. Zaelzer, C., Hua, P., Prager-Khoutorsky, M., Ciura, S., Voisin, D.L., Liedtke, W., and Bourque, C.W. (2015). DeltaN-TRPV1: A Molecular Co-detector of Body Temperature and Osmotic Stress. Cell Rep. *13*, 23–30.
12. Prager-Khoutorsky, M., Khoutorsky, A., and Bourque, C.W. (2014). Unique interweaved microtubule scaffold mediates osmosensory transduction via physical interaction with TRPV1. Neuron *83*, 866–878.
13. Zhang, Z., Kindrat, A.N., Sharif-Naeini, R., and Bourque, C.W. (2007). Actin filaments mediate mechanical gating during osmosensory transduction in

rat supraoptic nucleus neurons. J. Neurosci. *27*, 4008–4013. https://doi.org/10.1523/JNEUROSCI.3278-06.2007.

14. Zhang, Z., and Bourque, C.W. (2008). Amplification of transducer gain by angiotensin II-mediated enhancement of cortical actin density in osmosensory neurons. J. Neurosci. *28*, 9536–9544.
15. Barad, Z., Jacob-Tomas, S., Sobrero, A., Lean, G., Hicks, A.I., Yang, J., Choe, K.Y., and Prager-Khoutorsky, M. (2020). Unique Organization of actin cytoskeleton in magnocellular vasopressin neurons in normal conditions and in response to salt-loading. eNeuro *7*, 1–13. https://doi.org/10.1523/eneuro.0351-19.2020.
16. Chattipakorn, S.C., and McMahon, L.L. (2003). Strychnine-sensitive glycine receptors depress hyperexcitability in rat dentate gyrus. J. Neurophysiol. *89*, 1339–1342. https://doi.org/10.1152/jn.00908.2002.
17. Efremov, Y.M., Shimolina, L., Gulin, A., Ignatova, N., Gubina, M., Kuimova, M.K., Timashev, P.S., and Shirmanova, M.V. (2023). Correlation of Plasma Membrane Microviscosity and Cell Stiffness Revealed via Fluorescence-Lifetime Imaging and Atomic Force Microscopy. Cells *12*, 2583. https://doi.org/10.3390/cells12212583.
18. Shigemura, K., Kuribayashi-Shigetomi, K., Tanaka, R., Yamasaki, H., and Okajima, T. (2023). Mechanical properties of epithelial cells in domes investigated using atomic force microscopy. Front. Cell Dev. Biol. *11*, 1245296. https://doi.org/10.3389/fcell.2023.1245296.
19. Levi, D.I., Wyrosdic, J.C., Hicks, A.I., Andrade, M.A., Toney, G.M., Prager-Khoutorsky, M., and Bourque, C.W. (2021). High dietary salt amplifies osmoresponsiveness in vasopressin-releasing neurons. Cell Rep. *34*, 108866. https://doi.org/10.1016/j.celrep.2021.108866.
20. Prager-Khoutorsky, M., and Bourque, C.W. (2010). Osmosensation in vasopressin neurons: changing actin density to optimize function. Trends Neurosci. *33*, 76–83. https://doi.org/10.1016/j.tins.2009.11.004.
21. Zhang, Z., and Bourque, C.W. (2003). Osmometry in osmosensory neurons. Nat. Neurosci. *6*, 1021–1022. https://doi.org/10.1038/nn1124.nn1124.
22. Ciura, S., Liedtke, W., and Bourque, C.W. (2011). Hypertonicity sensing in organum vasculosum lamina terminalis neurons: a mechanical process involving TRPV1 but not TRPV4. J. Neurosci. *31*, 14669–14676. https://doi.org/10.1523/jneurosci.1420-11.2011.
23. Pinigin, K.V. (2022). Determination of Elastic Parameters of Lipid Membranes with Molecular Dynamics: A Review of Approaches and Theoretical Aspects. Membranes *12*, 1149. https://doi.org/10.3390/membranes12111149.
24. Prager-Khoutorsky, M. (2017). Mechanosensing in hypothalamic osmosensory neurons. Semin. Cell Dev. Biol. *71*, 13–21. https://doi.org/10.1016/j.semcdb.2017.06.006.

STAR★METHODS

KEY RESOURCES TABLE

REAGENT or RESOURCE	SOURCE	IDENTIFIER
Antibodies		
Anti β-actin mouse monoclonal antibody	Millipore Sigma	Cat#A5441 clone AC 15; RRID: AB_476744
Anti α-tubulin mouse monoclonal antibody	Millipore Sigma	Cat# CP06; RRID: AB_2617116
Anti TRPV1 rabbit polyclonal antibody	Alomone labs	Cat#ACC-030; RRID: AB_2313819
Goat anti-Rabbit IgG (H + L) Cross-Adsorbed Secondary Antibody, Alexa Fluor™ 488	Thermo Fisher Scientific	Cat# A-11008; RRID: AB_143165
Chemicals, peptides, and recombinant proteins		
CellBrite® Green Membrane Dye	Thermo Fisher Scientific	Cat#NC1136383
Spirochrome SiR-Actin kit	Cytoskeleton Inc.	Cat# CY-SC001
TRPV1/VR1 (extracellular) Blocking Peptide	Alomone labs	Cat#BLP-CC029
Alexa Fluor™ 488 Phalloidin	Thermo Fisher Scientific	Cat#A12379
DAPI	Thermo Fisher Scientific	Cat#D1306
Critical commercial assays		
Duolink® Proximity Ligation Assay	Millipore Sigma	the Duolink *In Situ* Detection Reagents Red (DUO92008); *In Situ* Red Starter Kit Mouse/Rabbit (DUO92101)
Experimental models: Organisms/strains		
Rat: Wistar	Charles River Laboratories	Crl: WI RRID: RGD_737929
Software and algorithms		
ImageJ	NIH	https://imagej.nih.gov/ij/ RRID: SCR_003070
OLYMPUS cellSens Dimension Desktop 2.2	OLYMPUS CORPORATION	https://evidentscientific.com/en/software/cellsens
GraphPad Prism v5.01	GraphPad Software, Inc.	www.graphpad.com RRID: SCR_002798
Sigmaplot v12.3	Systat Software, Inc.	Graffiti.com RRID: SCR_003210

EXPERIMENTAL MODEL AND STUDY PARTICIPANT DETAILS

Animals

All procedures were carried out under the approval of the Facility Animal Care Committee of McGill University (protocol AUP1190) and treated in strict accordance with the guidelines outlined by the Canadian Council on Animal Care (https://ccac.ca/). Male Wistar rats (4-8 weeks; Charles River Laboratories Inc. RRID: RGD_737929) were used throughout the study. All animals were kept under a standard 12/12 h light/dark cycle and housed in groups of 2. Food and water were provided *ad libitum*. All experiments were done during the light phase.

METHOD DETAILS

Preparation of isolated cells

Isolated cells were prepared as previously described (Prager-Khoutorsky et al. 2014). Briefly, rats were sacrificed by decapitation, and the brain was rapidly removed from the cranium and placed in chilled oxygenated (100% O_2) PIPES solution (pH 7.3) containing 120 mM NaCl, 5mM KCl, 1 mM $MgCl_2$, 10 mM PIPES, 1 mM $CaCl_2$, and 10 mM glucose (osmolality adjusted to 295 mosmol kg^{-1} using mannitol). Blocks of tissue containing the target nuclei (~1 mm^3) were removed using iridectomy scissors and placed in PIPES solution containing 0.7 mg/ml protease XIV (Sigma-Aldrich, St. Louis, U.S.A.) at 31°C for 30 min. Tissue blocks were then transferred to a protease-free PIPES solution, triturated using fire-polished Pasteur pipettes, and plated on glass-bottomed petri dishes.

Antibodies

Anti β-actin mouse monoclonal antibodies (catalog #A5441 clone AC 15; Millipore Sigma, 1:200). Anti α-tubulin mouse monoclonal antibody (DM1A, Millipore Sigma, 1:500). Anti TRPV1 rabbit polyclonal antibody (and the blocking peptide to verify its specificity, Alomone labs, Jerusalem, Israel, 1:200) directed against the C terminus of TRPV1. Secondary antibodies were fluorescently labeled and Alexa-conjugated (Alexa Fluor secondary antibodies, 488 nm, 568 nm, and 647 nm; 1:500; Thermofisher Scientific, St. Laurent, Canada).

In situ proximity ligation assay

Sites at which TRPV1 is in close proximity of tubulin or actin were detected using the Duolink *In Situ* Detection Reagents Red (DUO92008) and the *In Situ* Red Starter Kit Mouse/Rabbit (DUO92101) according to the manufacturer's instructions (#G9023; Sigma-Aldrich). Briefly, acutely isolated neurons were fixed and permeabilized, then primary antibodies against TRPV1 and α-tubulin or β-actin were applied at 4°C overnight. Duolink secondary antibodies conjugated to oligonucleotides were then added and incubated at 37°C for 1 h in a preheated humidified chamber. This was then followed by ligation and amplification using the kit's ligase and polymerase solution that also contained fluorescently labeled oligonucleotides. According to the manufacturer, signal is only generated if the two antigens are within 40 nm of each other. After this, samples were incubated in phalloidin conjugated to Alexa Fluor 488 (Invitrogen, Waltham, U.S.A.; 1:200) for 1 hour to stain for cortical f-actin, followed by a wash with PBS. Finally, samples were counterstained with DAPI (included in the mounting medium; DUO82040) and confocal images were captured using an FV 3000 microscope (60x, 194.3 nm XY 1.35 N.A.; FV3000 Olympus Canada Inc).

Membrane and actin probe staining and imaging

Live isolated cells in PIPES solution were treated with CellBrite membrane dye (Thermofisher Scientific; 1:200) and cell-permeable actin probes (Spirochrome SiR-Actin kit; Cytoskeleton Inc., Denver, U.S.A.; 1:100) for 30 minutes followed by a wash with HEPES solution. In dynamic hypertonicity experiments, live membrane-labeled isolated cells were exposed a hypertonic stimulus (+4.5 mM), hyper-adjusted with mannitol diluted in HEPES. Stacks of 4-10 confocal super-resolution images (z spacing: 0.32 μm) were acquired at 15 second intervals (60x; 89 nm XY 1.35 N.A.; FV 3000-OSR module; Olympus Canada Inc). For static experiments, isolated neurons were treated with either isotonic (300 mosmol/kg) or hypertonic solution (304.5 mosmol/kg) and fixed with 4% paraformaldehyde. Stacks of super-resolution confocal images were then collected as described above. Skeletonized membrane rendering was done in ImageJ software (Bethesda, U.S.A.).

Analysis of PLA puncta

Tubulin-TRPV1 proximity ligation assay (PLA) puncta were quantified based on their proximity to the actin cortex (counterstained with phalloidin). Puncta within 1 μm of the actin cortex that were above the threshold intensity (visible puncta with the lowest intensity in each image was measured to determine lower threshold) were counted.

3D membrane visualization

Stacks of super-resolution images were acquired from 4% paraformaldehyde-fixed, membrane-stained cells (CellBrite membrane dye, Thermofisher Scientific; 1:200) treated with isotonic or hypertonic solution. The stacks were deconvoluted using the constrained iterative module with 5 iterations and then 3D rendered using isosurface projection (Voxel View; Olympus cellSens Dimension Desktop 2.2, Olympus Canada Inc).

3D actin fenestrae analysis

Fenestrae were detected according to the following procedure. Stacks of confocal images encompassing entire ONs which were stained with fluorescent phalloidin were collected (60x objective; z-spacing 0.32 μm). The stacks were then 3D-rendered using 3D Viewer (surface display) and thresholded at 10 units above the mean cytoplasmic fluorescence intensity value. A smoothening factor of 15 was applied to the 3D mesh. The yielded actin fenestrae were then measured for length and width, the average of which was taken as mean diameter. Fenestrae density was determined by counting the number of fenestrae in a 10 x 10 μm region of interest on the top or bottom surface of the cell in the z axis.

Measurement of distance between PLA puncta and PM

To perform this analysis, the brightness and contrast of isolated ONs was optimized to visualize the outline of the PM relative to background. A line traced over this outline was taken to represent the skeletonized PM. In hypertonicity-treated ONs, actin fenestrae were associated with pit or non-pit PM domains. In pit PM domains, the estimated pre pit position (PPP) of the PM was arbitrarily drawn as an extension of the adjacent PM. The distance between the centre of PLA puncta and PM (isotonic or hypertonic non-pit) or estimated PPP (hypertonic pit) was measured in ImageJ.

QUANTIFICATION AND STATISTICAL ANALYSIS

All values in this study are reported as mean plus or minus the standard error of the mean (mean ± s.e.m.). Differences between groups were assessed using Sigmaplot 12.3 (Systat Software Inc. California, USA). The software first assessed normality of the

data distribution and equal variance between groups. When these conditions were not met, a suitable non-parametric test was performed. Significant differences were determined by One-way ANOVA, Tukey's Multiple Comparison, Mann Whitney, and Dunn's Multiple Comparison tests. Graphs were prepared using Prism 5.0 (GraphPad Software, Massachusetts, USA) which was also used to calculate and plot linear regressions. In all statistical comparisons, differences were considered significant when $p < 0.05$. * $P < 0.05$; ** $P < 0.01$; *** $P < 0.001$; ns, non-significant. Statistical details of experiments can be found in the results and figure legends.